Predicting pure amnestic mild cognitive impairment conversion to Alzheimer's disease using joint modeling of imaging and clinical data

V. Kebets [a,b], J. Richiardi [a], M. van Assche [a,b], R. Goldstein [a,b], M. van der Meulen [a], P. Vuilleumier [a], D. Van de Ville [a,c], F. Assal [a,b]

[a] *University of Geneva, Switzerland*
[b] *Geneva University Hospital, Switzerland*
[c] *Ecole Polytechnique Fédérale de Lausanne, Switzerland*
Email: Valeria.Kebets@unige.ch

***Abstract*—Predicting the conversion of amnestic mild cognitive impairment (aMCI) to Alzheimer's disease (AD) is a challenging problem for which machine learning could be of great use. In this work, we aim at assessing the independent and joint value of imaging (structural MRI, resting-state functional MRI (rsfMRI)) and clinical data in classifying stable versus progressive aMCI. Surprisingly, we found no previous studies using rsfMRI to predict conversion of MCI to AD. We use singular value decomposition as a feature extractor before combining modalities. We reach accuracies of up to 82% using rsfMRI, 86% using sMRI and rsfMRI combined, and 77% using a combination of all modalities.**

Keywords—Alzheimer's disease; amnestic mild cognitive impairment; magnetic resonance imaging; machine learning; singular value decomposition.

I. Introduction

The early diagnosis of Alzheimer's disease (AD) is of great importance since treatments will be most effective when administered in the early stages of the disease. Amnestic mild cognitive impairment (aMCI) patients have an increased risk of developing AD [1]; however, not all aMCI patients develop AD, as some may remain stable over time, revert to a normal cognitive state, or progress to another type of dementia [2]. It is thus crucial to identify those aMCI patients that will convert to AD. In this respect, machine learning holds vast potential.

Among different modalities used in the past few years to predict conversion of aMCI to AD, structural magnetic resonance imaging (sMRI) has probably shown the most consistent results. Prediction accuracies between 56-81% have been reported [3-9].

Functional connectivity changes in resting-state (rs) fMRI have also been reported throughout the progression from MCI to AD. These alterations were shown at the regional level (e.g. hippocampus [10]) but also within and between large-scale functional brain networks (e.g. default mode [11]). Surprisingly, we found no previous studies that have deployed pattern recognition tools on rsfMRI data to classify amnestic MCI converters (aMCI-c) versus amnestic MCI nonconverters (aMCI-nc).

Another approach to predict conversion is to use neuropsychological scores as features [12].

Finally, the availability of open multimodal datasets such as ADNI has shown that the full combination of several modalities, e.g. imaging and clinical data, may be the most promising method to accurately predict progression to AD, with classification accuracies reaching up to 89% [13-16].

In this work, we assess the classification performance of sMRI, rsfMRI and clinical measures, in distinguishing aMCI-c from aMCI-nc, using a random forest classifier, which does not suffer from feature scaling issues when combining different modalities [16]. We use singular value decomposition (SVD) as a feature extractor to identify low-dimensional components, which we subsequently use as features for classification.

II. Material and Methods

2.1 Subjects

We use baseline imaging (sMRI, rsfMRI) and clinical data from a local longitudinal study that follows pure aMCI patients until their potential conversion to AD. aMCI patients fulfilled Petersen's criteria [17], consisting of subjective memory complaint, objective memory impairment (informed by a score of 1.5 standard deviation (SD) below age- and education-adjusted norms on at least two memory subtests), no impairment in other cognitive domains (no more than one subtest in deficit), intact general cognitive function, no impairment in activities of daily living, and no dementia. At the time of the analysis, 11 aMCI had converted to AD, while 11 had not. The mean time of follow-up was 24 months (range: 0-50) and the mean time of conversion was 30 months (range: 11-68). Sociodemographic data are presented in **Table I;** two-sample t-tests show no difference between the two groups in age, gender or education.

2.2 Neuropsychological evaluation

We used z-scores of 13 neuropsychological tests for which population normative data were available: Dementia Rating Scale, immediate and delayed cued recall from the Grober-Buschke Memory Impairment Screen, Doors and People Test

978-1-4673-7145-2/15 $31.00 © 2015 IEEE
DOI 10.1109/PRNI.2015.23

(part A and B), Trail Making Test (part A and B), Stroop Test (interference score), Digit Span (forward and backward) from the Wechsler Memory Scale, Boston Naming Test, semantic and phonemic verbal fluency. References for these tests can be found in [18]. Missing scores that resulted from not completing a test because the patient was too impaired were replaced by a z-score corresponding to a percentile of 1% (3 MCI-c had respectively 5, 1 and 1 missing scores, while 2 MCI-nc had respectively 4 and 1 missing score). Notably, there was no significant difference in any neuropsychological test between the two groups at baseline.

TABLE I. SOCIODEMOGRAPHIC DATA

	MCI nonconverters	MCI converters	p-val
Age (mean±SD)	72.3 ± 9.2	71.9 ± 5.6	0.91
Gender (F/M)	4 / 7	7 / 4	0.22
Education (mean±SD)	12.7 ± 3.3	14.0 ± 3.8	0.41

2.3 Data acquisition

Two identical scanners, both 3T Siemens Trio TIM using a 32-channel head coil, were used to acquire the imaging data. 2 aMCI-c and 2 aMCI-nc were scanned in the first scanner, while the remaining subjects were scanned in the second one. Identical imaging parameters were used with both scanners. All subjects were scanned during a single session that included the resting-state functional images as well as the anatomical scan. In the resting-state paradigm, subjects were presented a white rotating cross on a grey background for 8:21 minutes. They were instructed to keep their eyes open and watch the cross rotate, while thinking of nothing in particular. Visual stimuli were presented on a projection screen inside the scanner using E-prime (E-prime 1.0, Psychology Software Tools Inc, Pittsburgh).

2.4 Imaging parameters

Whole brain functional images acquired during rest were collected using an EPI sequence (TR/TE=1100/27ms; flip angle = 90 degrees; PAT factor = 2; FOV = 240mm; matrix size = 64 x 64 pixels). We acquired 21 transversal slices sequentially with a 4.5 mm thickness and an interslice gap of 1.125 mm, yielding a voxel size of 3.8 x 3.8 x 5.6 mm. High-resolution whole brain anatomical scans were acquired with a T1-weighted, 3D sequence (MPRAGE; TR/TI/TE = 1900/900/2.32 ms; flip angle = 9 degrees; voxel dimensions = 0.9 mm isotropic; 256 x 256 x 192 voxels).

2.5 Structural MRI preprocessing

Structural data were preprocessed and analyzed using the VBM8 toolbox (http://dbm.neuro.uni-jena.de/vbm/) implemented in SPM8 (http://www.fil.ion.ucl.ac.uk/spm/). Anatomical scans were first segmented into grey matter (GM), white matter and cerebrospinal fluid using the *new segmentation* algorithm. GM images were warped to the MNI space, and a group GM template was created using DARTEL tools. GM images were then spatially normalized, modulated and smoothed with a 4mm full-width-at-half-maximum Gaussian filter. All voxels with a GM probability > 0.1 were used as features, making a training feature vector of size *(N-1)* x 401427.

2.6 Resting-state fMRI preprocessing and modeling

We followed the methodology described in previous work [19, 20] to preprocess the rsfMRI data and extract functional connectivity matrices. Briefly, after functional images were realigned, the mean image of the functional data was co-registered with the anatomical scan. A customized version of the IBASPM toolbox [21] was used to build an individual structural brain atlas for each subject, based on 2 different atlases (for comparison): the AAL structural atlas [22] and the Shirer ICA-derived functional atlas [23]. We selected 88 regions in the AAL atlas (whole atlas without cerebellum and pallidum) and all 90 regions for the Shirer atlas. The atlas was then mapped back onto the native resolution of the functional data, time series were linearly detrended, and region-averaged time series were extracted. These time series were Winsorized to the 95th percentile to increase robustness to outliers (e.g. spikes). The first 10 time points were discarded to ensure magnetization equilibrium, and 6 movement parameters were regressed out. Time courses were then filtered into frequency subbands using a wavelet transform (cubic orthogonal B-spline wavelets). The subband of interest for this study contained frequencies in the 0.03–0.06 Hz range, based on previous observations (not shown here). After computing pairwise Pearson correlations between all regions in the atlas, a correlation matrix (number of regions × number of regions) was obtained for each subject.

This functional connectivity matrix was used as the adjacency matrix of a connectivity graph, where each region corresponded to a vertex, and the strength of functional connectivity between two regions (a correlation coefficient) was encoded in the edge weight. We used direct graph embedding, in which the upper triangular part of the adjacency matrix is lexicographically organized in a vector representation. Our training feature vector is *(N-1)* x 3828 for the AAL atlas and *(N-1)* x 4005 for the Shirer atlas.

2.7 Singular value decomposition

In order to combine modalities and avoid needlessly increasing the dimensionality of our feature space, we first reduce the dimensionality of our different features matrices. While a common machine learning approach would be to use multiple kernel learning with one Gram matrix per modality, we wanted to try a tool from classical multivariate analysis, i.e. singular value decomposition.

Singular value decomposition (SVD) of a matrix $\mathbf{X}$ is a factorization into three matrices: $\mathbf{X} = \mathbf{USV}^{\mathbf{T}}$. The columns of $\mathbf{U}$ contain the principal components, $\mathbf{V}$ contains the loadings, and the matrix $\mathbf{S}$ is a diagonal with positive real numbers.

We used only the first column of $\mathbf{U}$ as features, which corresponds to the first principal component (PC1) and explains the biggest portion of variance. Another possibility would be to adaptively select an optimal number of PCs using nested cross-validation in each fold.

Classification using PC1 was conducted in a leave-one-subject-out cross-validation fashion: for each fold, SVD decomposition was first computed on each modality independently for *N-1* subjects, whose principal components (**U**) are multiplied by the diagonal (**S**) and then used for training. The initial data of the left-out subject are then projected on the loadings ($\mathbf{V^T}$) of the training data. Our training feature vector is thus *N-1* x 1.

For joint modeling, we simply perform SVD on each modality independently, and join them by concatenation.

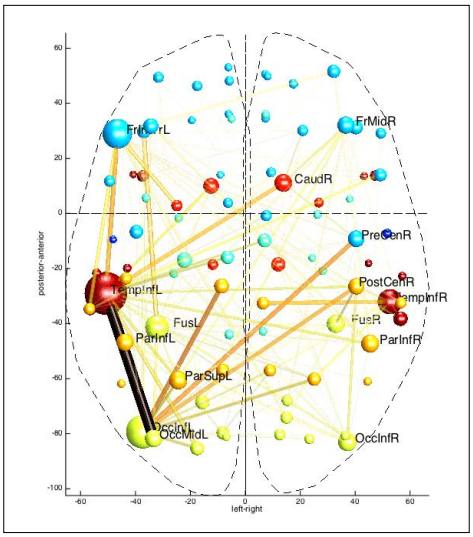

Fig. 1. The most discriminative rsfMRI connections in the AAL atlas. Spheres represent regions, and are colored according to the anatomical lobe to which they belong. Thicker lines correspond to connections that have higher Gini importance in the RF classifier.

2.8 Classification

A random forest (RF) classifier (using 501 trees), as implemented in Matlab (https://code.google.com/p/randomforest-matlab/) was used to discriminate between aMCI-c and aMCI-nc. One reason for using this classifier is that our different modalities have very different dynamic ranges, and RF is scale-insensitive. We note that we could also have used another classifier by suitably normalizing features in each modality.

We report accuracy, specificity, sensitivity, and area under the ROC curve (AUC). In order to evaluate the performance and generalization ability of our classifier, we chose a leave-one-subject-out cross-validation approach. We ran 1000 permutations to test for the significance of our accuracies.

III. Results

3.1 Classification with imaging data

Prediction accuracies obtained with sMRI and rsfMRI (using the AAL and Shirer atlases), either in high or low dimensions (SVD PC1), are presented in **Table II.** The most discriminative rsfMRI connections of the AAL atlas are shown in **Fig. 1**.

TABLE II. Prediction performance using imaging data

	Acc	Spec	Sens	AUC	p-val
sMRI data					
high dimensional	45%	36%	54%	0.34	n.s.
low dimensional	**77%**	73%	82%	0.79	0.014
rsfMRI data					
AAL					
high dimensional	**68%**	64%	73%	0.68	0.015
low dimensional	55%	45%	64%	0.53	n.s.
Shirer					
high dimensional	**82%**	82%	82%	0.79	0.002
low dimensional	**68%**	64%	73%	0.63	0.049

3.2 Classification with clinical data

Prediction accuracies obtained with neuropsychological z-scores were between 23% (Trail Making Test B) and 64% (Boston Naming Test); none of these accuracies were above chance level. When reducing all scores using SVD and taking the first component only, we reached 32% accuracy.

3.3 Classification with joint modalities

Prediction accuracies obtained with joint modalities computed via SVD are presented in **Table III.** We reached 77% using sMRI and clinical data, 86% using sMRI and rsfMRI, and 77% using sMRI+rsfMRI+clinical data.

TABLE III. Prediction performance using joint modalities

	Acc	Spec	Sens	AUC	p-val
sMRI-clinical	**82%**	82%	82%	0.74	0.004
rsfMRI (*AAL*) –clinical	45%	64%	27%	0.50	n.s.
rsfMRI (*Shirer*) –clinical	55%	64%	45%	0.56	n.s.
sMRI-rsfMRI (*AAL*)	**86%**	91%	82%	0.89	0.001
sMRI-rsfMRI (*Shirer*)	**86%**	91%	82%	0.88	0.001
sMRI-rsfMRI (*AAL*)-clinical	**77%**	82%	73%	0.84	0.009
sMRI-rsfMRI (*Shirer*)-clinical	**77%**	82%	73%	0.81	0.008

We further looked into the relative importance of each modality in the classification prediction, using Gini importance [24] computed by the RF. For joint sMRI-clinical data, sMRI was almost twice as important as clinical data (significant at $p<0.001$ using a t-test). For joint sMRI-rsfMRI-clinical data, sMRI data was more important than rsfMRI data, which in turn was more important than clinical data (all significant at $p<0.001$ using an F-test). The Gini importance of each modality for the joint modeling of all three modalities (sMRI-rsfMRI *(Shirer)*-clinical) is illustrated in **Fig. 2.**

IV. Discussion

While baseline clinical data does not allow predicting conversion of aMCI to AD, rsfMRI yields accuracies of up to 82% (consistent across 2 atlases). These findings are extremely promising, considering that no previous studies have deployed pattern recognition tools on rsfMRI for

conversion prediction. Using sMRI, we reach up to 77%; these results are in line with what is reported in the literature; however, it is important to note that most papers have used large datasets such as ADNI or AddNeuroMed. Nevertheless, smaller databases such as the one used by [25] have reached accuracies of up to 75%. The use of joint imaging and clinical modalities yields up to 77% accuracy, with imaging data weighting more than clinical data in the classifier's decision. The highest prediction accuracy that we reach is by combining both imaging modalities (86% accuracy). The fact that imaging data can accurately predict conversion of aMCI to AD, while clinical data do a poor job, may suggest that changes in the function and structure of the brain precede measurable cognitive deficits during the progression to disease.

An important limitation of this study is the small sample size, as the cohort we used comes from a small local longitudinal study. However, given this limitation, the predictive power obtained in this challenging question is all the more remarkable. Another limitation is the use of a group template during sMRI preprocessing, which could have induced knowledge about the test set in the training set.

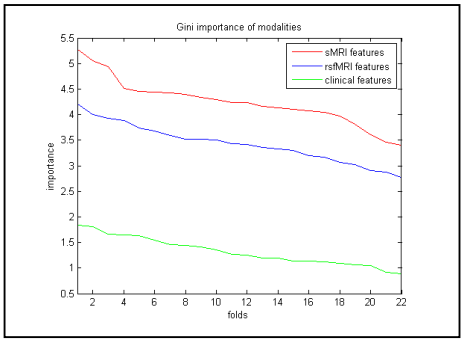

Fig. 2. Gini importance of sMRI, rsfMRI (Shirer atlas) and clinical features in the joint modeling of all three modalities, sorted in decreasing order within each modality.

ACKNOWLEDGMENTS

This work was supported by the Swiss National Science Foundation under grants 320030_138163 (to FA) and PP00P2-146318 (to DVDV), and by a Marie Curie International Outgoing Fellowship of the European Commission's 7th framework program (PIOF-GA-2011-299500, to JR). We also wish to thank the Swiss Society for Neuroscience for its travel fellowship that will allow VK to attend the workshop.

REFERENCES

1. Gauthier, S., et al., *Mild cognitive impairment.* Lancet, 2006. **367**(9518): p. 1262-70.
2. Ganguli, M., et al., *Mild cognitive impairment, amnestic type: an epidemiologic study.* Neurology, 2004. **63**(1): p. 115-21.
3. Leung, K.K., et al., *Increasing power to predict mild cognitive impairment conversion to Alzheimer's disease using hippocampal atrophy rate and statistical shape models.* Med Image Comput Comput Assist Interv, 2010. **13**(Pt 2): p. 125-32.
4. Misra, C., Y. Fan, and C. Davatzikos, *Baseline and longitudinal patterns of brain atrophy in MCI patients, and their use in prediction of short-term conversion to AD: results from ADNI.* Neuroimage, 2009. **44**(4): p. 1415-22.
5. Moradi, E., et al., *Machine learning framework for early MRI-based Alzheimer's conversion prediction in MCI subjects.* Neuroimage, 2015. **104**: p. 398-412.
6. Tang, X., et al., *Baseline shape diffeomorphometry patterns of subcortical and ventricular structures in predicting conversion of mild cognitive impairment to Alzheimer's disease.* J Alzheimers Dis, 2015. **44**(2): p. 599-611.
7. Wee, C.Y., et al., *Prediction of Alzheimer's disease and mild cognitive impairment using cortical morphological patterns.* Hum Brain Mapp, 2013. **34**(12): p. 3411-25.
8. Wolz, R., et al., *Multi-method analysis of MRI images in early diagnostics of Alzheimer's disease.* PLoS One, 2011. **6**(10): p. e25446.
9. Davatzikos, C., et al., *Prediction of MCI to AD conversion, via MRI, CSF biomarkers, and pattern classification.* Neurobiol Aging, 2011. **32**(12): p. 2322 e19-27.
10. Wang, Z., et al., *Baseline and longitudinal patterns of hippocampal connectivity in mild cognitive impairment: evidence from resting state fMRI.* J Neurol Sci, 2011. **309**(1-2): p. 79-85.
11. Yao, H., et al., *Longitudinal alteration of amygdalar functional connectivity in mild cognitive impairment subjects revealed by resting-state FMRI.* Brain Connect, 2014. **4**(5): p. 361-70.
12. Chapman, R.M., et al., *Predicting conversion from mild cognitive impairment to Alzheimer's disease using neuropsychological tests and multivariate methods.* J Clin Exp Neuropsychol, 2011. **33**(2): p. 187-99.
13. Cui, Y., et al., *Identification of conversion from mild cognitive impairment to Alzheimer's disease using multivariate predictors.* PLoS One, 2011. **6**(7): p. e21896.
14. Ewers, M., et al., *Prediction of conversion from mild cognitive impairment to Alzheimer's disease dementia based upon biomarkers and neuropsychological test performance.* Neurobiol Aging, 2012. **33**(7): p. 1203-14.
15. Hinrichs, C., et al., *Predictive markers for AD in a multi-modality framework: an analysis of MCI progression in the ADNI population.* Neuroimage, 2011. **55**(2): p. 574-89.
16. Segovia, F., et al., *Combining PET images and neuropsychological test data for automatic diagnosis of Alzheimer's disease.* PLoS One, 2014. **9**(2): p. e88687.
17. Petersen, R.C., *Mild cognitive impairment as a diagnostic entity.* J Intern Med, 2004. **256**(3): p. 183-94.
18. van der Meulen, M., et al., *Associative and semantic memory deficits in amnestic mild cognitive impairment as revealed by functional magnetic resonance imaging.* Cogn Behav Neurol, 2012. **25**(4): p. 195-215.
19. Richiardi, J., et al., *Decoding brain states from fMRI connectivity graphs.* Neuroimage, 2011. **56**(2): p. 616-26.
20. Richiardi, J., et al., *Classifying minimally disabled multiple sclerosis patients from resting state functional connectivity.* Neuroimage, 2012. **62**(3): p. 2021-33.
21. Alemán-Gómez, Y., L. Melie-García, and P. Valdés-Hernandez. *IBASPM: toolbox for automatic parcellation of brain structures*. in *Annual Meeting of the Organization for Human Brain Mapping*. 2006. Florence, Italy.
22. Tzourio-Mazoyer, N., et al., *Automated anatomical labeling of activations in SPM using a macroscopic anatomical parcellation of the MNI MRI single-subject brain.* Neuroimage, 2002. **15**(1): p. 273-89.
23. Shirer, W.R., et al., *Decoding subject-driven cognitive states with whole-brain connectivity patterns.* Cereb Cortex, 2012. **22**(1): p. 158-65.
24. Breiman, L., *Random Forests.* Machine Learning, 2001. **45**(1): p. 5-32.
25. Plant, C., et al., *Automated detection of brain atrophy patterns based on MRI for the prediction of Alzheimer's disease.* Neuroimage, 2010. **50**(1): p. 162-74.